Catalysis Today 168 (2011) 80–85

Contents lists available at ScienceDirect

Catalysis Today

journal homepage: www.elsevier.com/locate/cattod

Influence of synthesis parameters on the catalytic activity of hierarchical SAPO-5 in space-demanding alkylation reactions

Nadiya Danilina, Stefano A. Castelanelli, Ekaterina Troussard, Jeroen A. van Bokhoven*

ETH Zurich, Institute for Chemical and Bioengineering, Wolfgang-Pauli-Str. 10, 8093 Zurich, Switzerland

ARTICLE INFO

Article history:
Received 20 October 2010
Received in revised form
21 December 2010
Accepted 26 January 2011
Available online 2 March 2011

Keywords:
SAPO-5
Hierarchical
Mesoporous
Alkylation
Amorphous silica-alumina

ABSTRACT

Hierarchical SAPO-5 catalysts with a bimodal pore system were synthesized and characterized with XRD, Al and Si AAS, N_2 physisorption, ^{27}Al and ^{29}Si MAS NMR, and temperature-programmed decomposition of *n*-propylamine. The effect of silicon source, silicon content, and amount of mesopore-directing agent (TPHAC) was studied. XRD showed that the crystallization of the SAPO-5 structure is strongly affected by the silicon source. Si AAS and ^{29}Si MAS NMR showed that higher silicon content in the synthesis mixture leads to higher silicon concentration in the bulk, whereas the amount of Si in the SAPO framework reaches a limit of 2.8 wt%. N_2 physisorption showed that the samples possess micro- and mesoporosity with a broad pore size distribution. Higher TPHAC content in the synthesis mixture did not lead to higher mesopore volume. The catalytic performance of the hierarchical H-SAPO-5 samples was studied in the alkylation of benzene and cyclohexylbenzene with benzyl alcohol and compared to that of microporous H-SAPO-5, zeolite H-Y, and amorphous silica-alumina. There were indications that amorphous phase, possibly present in the mesoporous samples, contributes to their catalytic activity. This might be an important issue for catalysis over hierarchical materials in general.

1. Introduction

In the family of aluminophosphate (ALPO)-based molecular sieves, silicoaluminophosphates (SAPOs) have considerable potential as acidic catalyst for the conversion of hydrocarbons. For example, microporous SAPO-5 is active in cumene synthesis [1], xylene isomerization [2], toluene alkylation by methanol [3], isopropylation of benzene [4], transalkylation of toluene with trimethylbenzenes [5], and many other reactions.

The acidity of SAPO results from the incorporation of Si^{4+} in the ALPO framework. Three main mechanisms for the incorporation of silicon were proposed in the literature: the so-called SM1, SM2, and SM3 [6]. The SM1-mechanism foresees the substitution of Al^{3+} ions by Si^{4+}, SM2 describes the substitution of P^{5+} by Si^{4+}, and SM3—the simultaneous occupation of both Al^{3+} and P^{5+} sites by Si^{4+}. Until now, there is no evidence of the formation of Si–O–P bonds (SM1). The SM2-type substitution leads to generation of isolated Brønsted acid sites, and SM3 to the formation of silicon islands with Si–OH groups at their borders.

Besides the presence of acidity, the accessibility of the acid sites is an important factor for the conversion of bulky molecules. Mesoporous or hierarchical SAPOs could offer more space for bulky molecules to diffuse and react. The most important methods to synthesize mesoporous zeolites and zeotypes are soft-templating [7], hard-templating [8], pillaring/delamination [9], post-synthesis treatment [10], and use of zeolite seeds as precursors in the preparation of mesoporous structures [11]. Using a soft template, enables the control of the shape and size of the solid and its pore system. Mesoporous zeolites, which have the most desirable properties for catalysis, such as high crystallinity, narrow pore size distribution, uniform pores, hydrothermal stability, and zeolite-like acidity, have been reported [12–14].

Recently, we have studied the incorporation of mesopores in SAPO-5 by applying different synthesis strategies [15]. The material with the best textural and catalytic properties in acid-catalyzed alkylation reactions was obtained by using cyclohexylamine to maintain the microporosity and a soft template with a silicon-containing head-group (TPHAC) [16] for the generation of mesopores. In order to optimize the catalytic performance of this hierarchical SAPO-5 material, we performed syntheses, where we systematically varied the silicon source, silicon content, and the amount of mesopore-directing agent in the reaction mixture. The phase-purest samples, preselected based on the results of the X-ray diffraction (XRD), were characterized with atomic absorption spectroscopy (AAS), nitrogen physisorption, ^{29}Si magic-angle spinning (MAS) nuclear magnetic resonance (NMR) spectroscopy, and temperature-programmed decomposition (TPD) of *n*-propylamine.

* Corresponding author. Tel.: +41 44 632 55 42/56 310 50 46.
E-mail address: j.a.vanbokhoven@chem.ethz.ch (J.A. van Bokhoven).

0920-5861/$ – see front matter © 2011 Elsevier B.V. All rights reserved.
doi:10.1016/j.cattod.2011.01.042

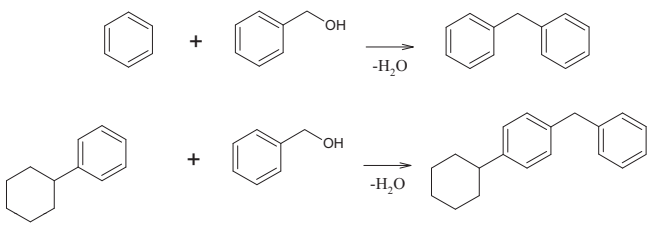

Scheme 1. Schematic representation of the alkylation of benzene or cyclohexylbenzene with benzyl alcohol.

They were also tested in alkylation of benzene and cyclohexylbenzene with benzyl alcohol to evaluate their catalytic properties in the conversion of bulky molecules. Microporous SAPO-5, zeolite H-Y, and amorphous silica-alumina (ASA) were used as references for the catalytic performance (Scheme 1).

2. Experimental

2.1. Catalysts

2.1.1. Mesoporous SAPO-5

Mesoporous SAPO-5 (mSAPO5) with a bimodal porosity was synthesized using cyclohexylamine (CHA) as a micropore-directing template and [3-(trimethoxysilyl)propyl]hexadecyldimethylammonium chloride (TPHAC) as a mesoporogene. The synthesis procedure of TPHAC and mSAPO-5 is described elsewhere [15,16]. The silicon source, silicon content, and TPHAC content were systematically varied. Table 1 summarizes the synthesis conditions.

2.1.1.1. Variation of silicon source. Four different silicon sources were tested for the synthesis of the mesoporous SAPO-5: fumed silica Cab-osil M-5 (Riedel-de-Haën), tetraethylorthosilicate (TEOS, Fluka), Ludox AS 40 (Aldrich), and water glass (sodium silicate solution, Merck). According to the synthesis procedure described before [15], one equivalent of silicon was added to the mixture resulting in a gel with the molar ratio Al:P:Si of 1:1:1. The samples were named mSAPO5, mSAPO5-teos, mSAPO5-lud, and mSAPO5-wg, respectively.

2.1.1.2. Variation of silicon content. Samples with three different silicon contents in the gel were prepared using fumed silica as silicon source (vide supra). The synthesis gels of mSAPO5, mSAPO5-0.5, and mSAPO5-0.25 had the molar composition Al:P:Si of 1:1:1, 1:1:0.5, and 1:1:0.25, respectively.

2.1.1.3. Variation of TPHAC content. Samples with three different contents of TPHAC were prepared from a gel with the molar ratio Al:P:Si of 1:1:1 using fumed silica as silicon source. The amounts of TPHAC added to the mixture were 1.91 g, 2.87 g, and 3.82 g, respectively, resulting in a gel with TPHAC:Al molar ratio of 0.018:1, 0.027:1, and 0.036:1. The samples were named mSAPO5, mSAPO5-T27, and mSAPO5-T36, respectively.

Table 1
Synthesis conditions of mSAPO5 samples.

Sample	Si source	Molar Al:P:Si	Molar TPHAC:Al
mSAPO5	Fumed silica	1:1:1	0.018
mSAPO5-teos	Tetraethylorthosilicate	1:1:1	0.018
mSAPO5-lud	Ludox AS 40	1:1:1	0.018
mSAPO5-wg	Sodium silicate	1:1:1	0.018
mSAPO5-0.25	Fumed silica	1:1:0.25	0.018
mSAPO5-0.5	Fumed silica	1:1:0.5	0.018
mSAPO5-T27	Fumed silica	1:1:1	0.027
mSAPO5-T36	Fumed silica	1:1:1	0.036

All samples were recovered by filtration, washed with 2 L of deionized water, dried at room temperature overnight, and calcined in air at 823 K for 20 h to remove the template. The samples mSAPO5, mSAPO5-0.5, and mSAPO5-T36 were ion-exchanged three times with 1 M NH_4NO_3 (Fluka, >99%) for 2 h at 348 K and calcined in nitrogen at 723 K for 4 h to give H-mSAPO5, H-mSAPO5-0.5, and H-mSAPO5-T36, respectively.

2.1.2. Reference catalysts

Microporous SAPO-5 was hydrothermally synthesized from a gel consisting of Al_2O_3:P_2O_5:0.24SiO_2:0.15CHA:20H_2O. The exact synthesis procedure was described elsewhere [15]. H-Y (CBV600, H-USY, Si/Al = 2.6) was obtained from Zeolyst International, USA. Amorphous silica-alumina (ASA, 11 wt% Al) was provided by Shell.

2.2. Characterization

X-ray powder diffraction (XRD) was conducted on a STOE STADI-P2 diffractometer in transmission mode using a flat sample holder and Ge-monochromated Cu Kα_1 radiation. The instrument was equipped with a position-sensitive detector with a resolution of $\sim 0.01^\circ$ in 2θ.

Nitrogen sorption measurements were performed at the temperature of liquid nitrogen on a Tristar 3000 apparatus of Micromeritics. Prior to the measurements, the samples were degassed at 10 mPa and 523 K for at least 2 h. The surface area was determined by the BET method; the *t*-plot method was used to determine the specific pore volume and the external surface area.

Atomic absorption spectroscopy (AAS) was performed on a Varian SpectrAA 220 FS spectrometer to determine elemental constitution. The samples were dissolved in an HF/HNO_3/water matrix overnight. Quantification of the aluminum content was done by the standard addition method. For silicon, individual calibration curves were measured and used for quantification.

^{29}Si magic-angle spinning nuclear magnetic resonance (MAS NMR) experiments were carried out on a Bruker 500 NMR spectrometer using a 4 mm probe-head. The relaxation delay was 10 s. All spectra were obtained at a spinning speed of 8 kHz. The chemical shifts were referenced to octakis-(trimethylsiloxy)silsesquioxane.

Scanning transmission electron micrographs (STEM) were obtained on a Tecnai F30 microscope operating with a field-emission cathode at 300 kV. High-angle annular dark-field (HAADF) detector and energy-dispersive X-ray (EDX) detectors were used. The sample was ground, dispersed in ethanol, and deposited on a holey carbon film supported on a copper grid.

For the temperature-programmed decomposition of *n*-propylamine with thermogravimetric analysis (TPD–TGA), approximately 20 mg sample were activated overnight at a pressure below 10^{-4} mPa by heating to 723 K with a ramp of 2 K/min. The sample was then exposed to *n*-propylamine at 473 K for 2 h and cooled to room temperature. The sample was evacuated for about 2 h to remove physisorbed *n*-propylamine. The thermogravimetric decomposition of *n*-propylamine was performed with a heating rate of 10 K/min and in a flow of 20 ml/min Ar in a Mettler Toledo TGA/SDTA851e instrument. The amount of decomposed *n*-propylamine was obtained from the mass change in the TGA curves between 573 and 650 K.

2.3. Catalytic tests

Alkylation of benzene (Acros, 99.7%) or cyclohexylbenzene (Fluka, 97%) with benzyl alcohol (Aldrich, 99.8%) were performed in a batch reactor (25 ml Berghof autoclaves BR-25) at a pressure between 25 and 27 bar and at 433 K. The reaction mixture for benzene alkylation contained 15 g (195 mmol) benzene, 0.26 g (2.4 mmol) benzyl alcohol, and 0.1 g catalyst. In case of cyclohexyl-

benzene alkylation, 15 g (95 mmol) cyclohexylbenzene was reacted with 0.13 g (1.2 mmol) benzyl alcohol over 0.05 g catalyst. The molar ratio of benzene, respectively cyclohexylbenzene, to benzyl alcohol was about 80. 0.08 g (0.71 mmol) ethylcyclohexane (Acros 99+%) was added to the reaction mixture as internal standard. Small liquid samples were taken after 0, 30, 60, 120, and 210 min and analyzed using a GC–MS equipped with a capillary HP-5MS (Agilent Technologies) column.

3. Results

3.1. Synthesis and characterization

Figure S1 (supporting information) shows XRD of all synthesized samples. Figure S1a shows XRD of the samples synthesized by varying the silicon source and the simulated diffractograms of AFI and CRI [17]. Only mSAPO5, synthesized with fumed silica, revealed a relatively pure AFI pattern. mSAPO5-teos, mSAPO5-lud, and mSAPO5-wg contained considerable amount of CRI (40–90%, estimated based on the most intensive reflection). Figure S1b shows XRD of mSAPO5 samples synthesized with different amount of fumed silica and mesopore-directing agent. mSAPO5-0.5 and mSAPO5-T36 were relatively pure crystalline AFI, whereas mSAPO5-0.25 and mSAPO5-T27 contained 40–55% CRI. Figure 1 shows XRD of the microporous SAPO-5, mSAPO5, mSAPO5-0.5, and mSAPO5-T36, which were used for further characterization, and a simulated diffractogram of the AFI structure. The samples showed sharp reflections over the whole 2θ range, indicating that they contained a crystalline phase; it corresponded to the AFI structure. Small amount of CRI impurities (22° 2θ) was observed. No reflections were observed in the 2θ range between 2 and 5° 2θ, indicating that the samples did not contain regular, uniform mesopores.

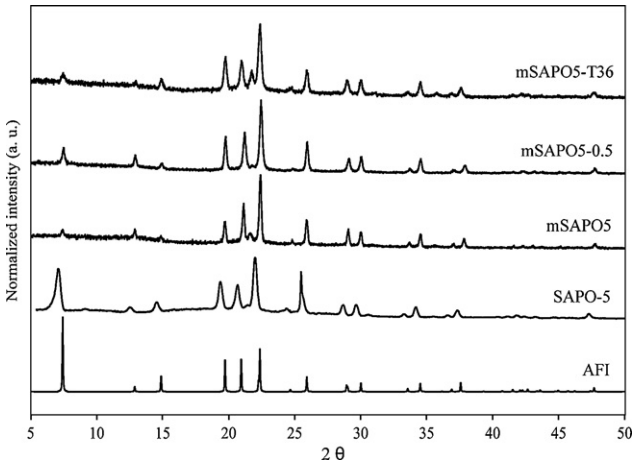

Fig. 1. XRD of SAPO-5, mSAPO5, mSAPO5-0.5, and mSAPO5-T36 and a simulated pattern of AFI.

Table 2 gives the results of elemental analysis, the deconvolution of ^{29}Si MAS NMR spectra, nitrogen physisorption, and the amount of decomposed *n*-propylamine (TPD–TGA) for the samples H-mSAPO5, H-mSAPO5-0.5, H-mSAPO5-T36, the microporous H-SAPO-5, H-Y, and ASA. For the H-mSAPO5 samples, the silicon concentration in the bulk was high and in good agreement with the amount of silicon in the reaction mixture: H-mSAPO5 and H-mSAPO5-T36, which were synthesized with one silicon equivalent, showed silicon content higher than 10 wt%, whereas H-mSAPO5-0.5, which was synthesized with 0.5 silicon equivalents, contained 7.1 wt% silicon. Nevertheless, the concentration of silicon in the SAPO domain was almost the same in all three samples, around 2.7 wt%. This is slightly lower than the silicon content in the frameworks of H-SAPO-5 and H-Y, which were used as references for the catalytic performance.

For the mesoporous H-mSAPO5 samples, the BET and the external surface areas as well as the micro- and mesoporous volumes were similar. The external surface area was relatively high, between 100 and 140 m^2/g (40–55% of the BET surface area). High micro- and mesoporous volume indicated the presence of bimodal porosity. Compared to microporous H-SAPO-5, the mesoporous samples showed lower BET surface area and microporous volume, whereas the mesoporous volume and external surface area were higher.

The number of Brønsted acid sites, determined with TPD-TGA of *n*-propylamine, ranged between 0.48 and 0.83 mmol/g for the SAPO-5 samples. It was higher for H-mSAPO-5, H-SAPO-5, H-mSAPO5-0.5, and lower for H-mSAPO5-T36. H-Y contained 1.57 mmol/g Brønsted acid sites and ASA −0.02 mmol/g.

Nitrogen sorption isotherms (Figure S2a, supporting information) of the mesoporous samples were also very similar and contained a hysteresis of type IV generated by capillary condensation in the meso- and macropores. The hysteresis did not contain a sharp step, and its shape indicated that the samples did not contain ordered mesopores. The strongest increase in adsorbed volume occurred at high partial pressure (0.9 p/p_0). The pore size distribution, determined from the desorption branch of the isotherm, is shown on Figure S2b (supporting information). All three samples showed a narrow and intense peak around 3.8 nm, which is attributed to the closing of the hysteresis loop at about $p/p_0 = 0.45$. Microporous H-SAPO-5 did not show any significant presence of mesopores, whereas pores between 5 and 60 nm were observed for the mesoporous materials.

The ^{29}Si MAS NMR spectra (Figure S3) of H-mSAPO5, H-mSAPO5-0.5, and H-mSAPO5-T36 were broad and asymmetric, indicating the presence of different silicon species. We assign the peak at about −90 ppm to silicon atoms located in the SAPO domain. The resonances at lower chemical shifts represented silicon located in the aluminosilicate region of the sample [18]. The percentage of silicon in the SAPO domain was always less than 50%, indicating that only a moderate part of silicon was effectively incorporated

Table 2
Characteristics of SAPO-5, mSAPO5 samples, H-Y, and ASA.

Sample	Si_{bulk}[a] (wt%)	Si_{fr}[b] (wt%)	S_{BET} (m^2/g)	S_{ext} (m^2/g)	V_{micro} (cm^3/g)	V_{meso} (cm^3/g)	*n*-PA[c] (mmol/g)
H-SAPO-5	5.6	3.3	325	95	0.10	0.12	0.79
H-mSAPO5	13.3	2.7	235	110	0.05	0.88	0.83
H-mSAPO5-0.5	7.1	2.8	245	135	0.06	1.05	0.76
H-mSAPO5-T36	11.0	2.7	240	100	0.04	0.91	0.48
H-Y	3.3	3.3	495	60	0.18	0.10	1.57
ASA	n.d.[d]	–	585	585	0	0.78	0.02

[a] Determined by AAS.
[b] Si in the framework, determined from the deconvolution of ^{29}Si MAS NMR spectra.
[c] *n*-Propylamine.
[d] Not determined.

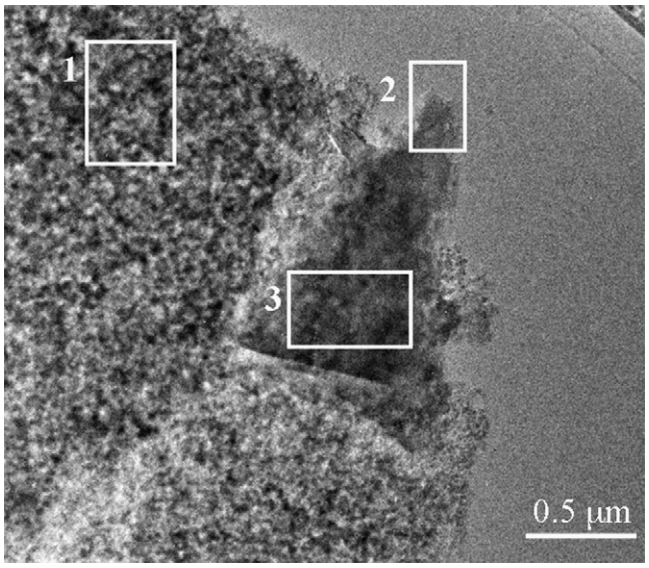

Fig. 2. STEM of mSAPO5: rectangle 1 – silicon-rich phase; rectangles 2 and 3 – SAPO crystal.

in the SAPO framework as isolated Si^{4+} via the SM2-mechanism [6,19].

SEM and TEM of SAPO-5 and mSAPO5 have been already shown elsewhere [15]. Intra- and interparticle mesopores were observed for the mesoporous sample. Fig. 2 shows a STEM image of mSAPO5. A part of a crystal (rectangles 2 and 3) and an amorphous-looking phase (rectangle 1) were distinguished. The EDX analysis of these areas showed that the ratio of Si:Al:P in the rectangle 1 is 35:4:1, in the rectangle 2, 7:19:12, and in the rectangle 3, 28:39:27. The phase 1 is rich in silicon, the rectangles 2 and 3 most probably correspond to the SAPO-5 crystal. These results fortify the suggestion that mSAPO5 samples contain several different phases.

3.2. Catalytic experiments

Fig. 3 shows the conversion as function of time in the alkylation of benzene (a) and cyclohexylbenzene (b) with benzyl alcohol for the microporous H-SAPO-5, the hierarchical H-mSAPO5, H-mSAPO5-0.5, and H-mSAPO5-T36 as well as for H-Y and ASA. All mesoporous materials showed similar activity in both reactions and were more active than the microporous H-SAPO-5. In the alkylation of benzene, the initial activity of the mesoporous samples was very high, and 100% conversion were already achieved after 60 min of reaction over H-mSAPO. The microporous SAPO-5 showed lower initial activity, and the conversion after 60 min was only 35%. H-Y was even less active: after 60 min, the conversion was 19%. However, ASA showed a profile very similar to that of mesoporous H-mSAPO5 samples. The conversion reached 100% after 60 min.

The activity in the alkylation of cyclohexylbenzene was lower than in the alkylation of benzene for all samples. Over the mesoporous samples, full conversion of benzyl alcohol (BA) was reached after about 210 min. Over the microporous H-SAPO-5, a maximum of 18% conversion was reached. Over H-Y, no benzyl alcohol was converted. The conversion plot of ASA was again very similar to that of H-mSAPO5 samples, 100% benzyl alcohol were converted after 210 min.

Table 3 gives the conversions of benzyl alcohol and the selectivity to diphenylmethane (DPM), respectively cyclohexylbenzyl benzene (CHBB) after 30 min. The mesoporous materials showed high conversion of benzyl alcohol (66–91%) with 100% selective formation of diphenylmethane, while over the microporous H-SAPO-5, only 18% of benzyl alcohol were converted, and the selectivity to DPM was 93%. Other products formed were diphenylether and 1,1,2-triphenylethane. Over H-Y, 4% benzyl alco-

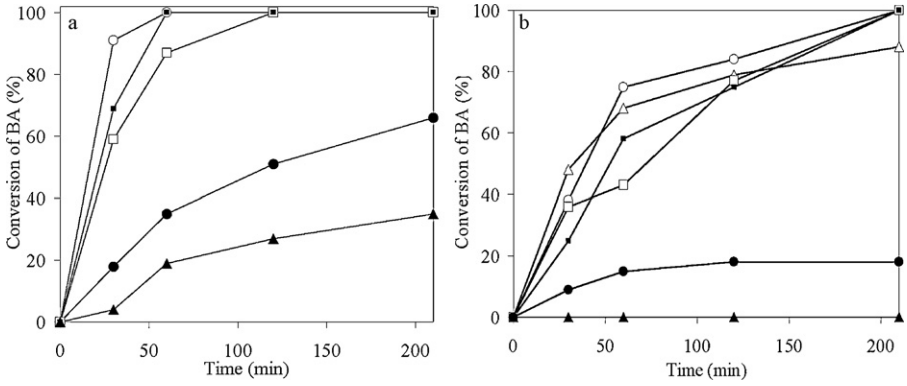

Fig. 3. Conversion of benzyl alcohol vs. time (a) in the alkylation of benzene and (b) cyclohexylbenzene with benzyl alcohol over H-SAPO-5 (●), H-mSAPO5 (○), H-mSAPO5-0.5 (△), H-mSAPO5-T36 (□), H-Y (▲), and ASA (■).

Table 3
Results of the alkylation of benzene and cyclohexylbenzene with benzyl alcohol after 30 min of reaction.

Sample	Benzene		Cyclohexylbenzene	
	X_{BA}[a] (%)	Selectivity to DPM[b] (%)	X_{BA} (%)	Selectivity to CHBB[c] (%)
H-SAPO-5	18	93	9	0
H-mSAPO5	91	100	38	21
H-mSAPO5-0.5	66	100	48	25
H-mSAPO5-T36	66	100	36	45
H-Y	4	100	0	–
ASA	69	100	25	45

[a] Conversion of benzyl alcohol.
[b] Diphenylmethane.
[c] Cyclohexylbenzyl benzene.

hol were converted; only DPM was detected in the product mixture. Over ASA, 69% were converted with 100% selectivity to DPM.

In the alkylation of cyclohexylbenzene, the most abundant product was benzene, which, most probably, resulted from the cracking of the alkylation product. Over the microporous H-SAPO-5, 9% benzyl alcohol were converted, and only benzene was observed as a product. Over the H-mSAPO5 samples, 36–48% benzyl alcohol was converted. 21–45% Cyclohexylbenzyl benzene were formed, whereas the highest selectivity was observed over H-mSAPO5-T36. No benzyl alcohol was converted over H-Y. Over ASA, 25% conversion were reached with a selectivity of 45% to cyclohexylbenzyl benzene.

4. Discussion

The crystallization of SAPO-5 depended strongly on the synthesis parameters. By varying the silicon source, its amount, and the amount of the mesopore-directing agent, products of different degree of crystallinity and with different amounts of crystobalite (CRI) were obtained. The formation of CRI, a siliceous crystalline phase, originated most probably from the high concentration of silicon in the reaction mixtures. CRI was the main product when using TEOS as a silicon source, whereas almost pure AFI was obtained with Cab-osil. Ludox AS40 gave a one-to-one mixture of AFI and CRI. Cab-osil is composed of solid silica nanoparticles, Ludox AS40 is a suspension of silica nanoparticles, TEOS is an organic source, and water glass is an inorganic material. Their different chemical nature leads to different dissolution behaviour and to mixtures with different homogeneity and pH, which affect the formation of different structures. The best result, i.e. the product with the lowest content of CRI impurity, was obtained with Cab-osil, which was, therefore, used for every further synthesis. The formation of AFI structure is similarly affected by the amount of silicon in the reaction mixture [25]. The sample with 0.5 silicon equivalents showed almost no CRI, whereas increasing and decreasing the silicon content led to the formation of the silicon-rich phase. The silicon concentration in the bulk correlated well with the silicon amount in the synthesis mixture, whereas no direct proportion between the silicon amount in the reaction mixture and the silicon concentration in the SAPO domain was observed. The amount of isolated Si^{4+} in the SAPO framework reached a constant value of about 2.7 wt% irrespective of the amount of silicon in the synthesis mixture. The substitution pattern for silicon in SAPO molecular sieves is known to be sensitive to many synthesis parameters, such as total silicon content, template/Al_2O_3 ratio, P_2O_5/Al_2O_3 ratio, pH, crystallization time, and temperature [20–22]. In general, with increasing amount of silicon in the synthesis gel, the content of the aluminosilicate domain increases [19]. At 0.28 equivalents of silicon in the framework, about 25% of it may have a zeolitic environment.

No direct proportion between the amount of the mesopore-directing agent (TPHAC) in the reaction mixture and the mesoporous volume was observed. This observation contradicts the results obtained by varying the amount of TPHAC in the synthesis of hierarchical ALPO-5 [7]. However, the mechanism of the incorporation of TPHAC might be strongly influenced by the presence of large amount of silicon in the synthesis mixture.

Hierarchical mSAPO5, mSAPO5-0.5, and mSAPO5-T36, obtained with Cab-osil as silicon source, represented a series of samples with two different silicon contents and synthesized with two different amounts of TPHAC. All three samples were crystalline SAPO-5 with micro- and mesoporosity with a broad pore size distribution. Interestingly, the BET surface area and the microporous volume were lower compared to the microporous material. The silicon concentration in the bulk was high and in good agreement with the amount of silicon equivalents used for the synthesis. Only a small part of this silicon was effectively incorporated into the aluminophosphate framework as isolated Si^{4+}. The rest of it was present in a phase with different aluminum coordination shells [23]. It is difficult to establish the exact nature of these species. XRD patterns clearly show the presence of a second crystalline phase, CRI, which is purely siliceous. However, its amount was too little to explain the high concentration of silicon in the aluminosilicate domain and the lower BET surface area and microporous volume. Based on the results of ^{29}Si MAS NMR and EDX/STEM, we suggest that the mesoporous mSAPO5 samples contain an additional amorphous phase, which could be amorphous silica alumina and/or an amorphous silicoaluminophosphate.

The role of the enhanced porosity was revealed by space-demanding alkylation of benzene and cyclohexylbenzene with benzene alcohol. Although it had almost the same number and strength of Brønsted acid sites as its microporous analogue (except of H-mSAPO5-T36), H-mSAPO5 samples were roughly three times more active than H-SAPO-5. This significant difference in catalytic activity indicates that the reaction occurs in the mesoporous domain, in agreement with the large external surface area. The presence of very bulky products also indicates that at least a part of the reaction takes place at the external surface. Zeolite H-Y, which has pores of dimensions similar to AFI (AFI: 0.73 nm × 0.73 nm, FAU: 0.74 nm × 0.74 nm), performed much worse, showing considerably lower conversions in both reactions. The catalytic performance of ASA instead was very similar to that of hierarchical SAPO-5 samples.

There are numerous publications on the catalytic performance of hierarchical materials in acid-catalyzed reactions, e.g. alkylation reactions [13,23–29]. However, to the best of our knowledge, the catalytic activity of hierarchical materials is rarely [13] compared with that of their amorphous analogues. As the amorphous phase is difficult to characterize, qualitatively and quantitatively; and indication of its presence and contribution to the catalytic activity of the hierarchical material can be only obtained by using the amorphous analogue as a reference during catalytic testing. In the paper of Sun and Prins [13], the catalytic activity of hierarchical ZSM-5 in alkylation of benzene with benzyl alcohol is compared to that of microporous ZSM-5 and amorphous silica-alumina (ASA). The conversion of benzyl alcohol after 10 h of reaction at 353 K was 10% over the microporous ZSM-5, 32% over ASA, and 98% over the hierarchical ZSM-5.

The mesoporous nature of H-mSAPO5 samples, which enables better transport of reactants and products into and out of the pores, certainly contributed to the observed high activity [7,17,18]. However, the improved activity could also be due to the presence of the amorphous phase. This results show the importance of the characterization of the amorphous debris in hierarchical zeolites and comparison of their catalytic properties with those of amorphous silica-alumina.

5. Conclusion

Crystalline hierarchical SAPO-5 with micro- and mesopores and a broad pore size distribution was synthesized. The influence of the amount of template, silicon source, and its content were investigated. Higher TPHAC content in the synthesis mixture did not result in materials with higher mesoporous volume. The formation of a crystalline mSAPO5 was strongly affected by the silicon source used. The material with the lowest amount of crystalline impurities was obtained with fumed silica. Higher silicon content in the synthesis mixture led to higher silicon concentration in the bulk. However, the amount of isolated Si^{4+} incorporated in the SAPO framework was lower than that in the bulk and was the same for all mesoporous SAPO. This and EDX/STEM analysis suggest the presence of an amorphous phase in the final hierarchical

SAPO materials, which could be amorphous silica-alumina and/or an amorphous silicoaluminophosphate.

Modification of microporous SAPO led to significant improvement of the catalytic properties in the alkylation of benzene and cyclohexylbenzene with benzyl alcohol. At the same time the catalytic behavior of amorphous silica-alumina showed similar results. This suggests that the presence of amorphous phase in the resulting materials might play significant role in the catalytic process. These insights might be of interest for the application of hierarchical materials in catalysis in general.

Acknowledgements

The work was supported by the Swiss National Science Foundation. We thank Dr. Frank Krumeich and the Electron Microscopy of the ETH Zurich (EMEZ) for the electron microscopy measurements.

Appendix A. Supplementary data

Supplementary data associated with this article can be found, in the online version, at doi:10.1016/j.cattod.2011.01.042.

References

[1] I.I. Ivanova, N. Dumont, Z. Gabelica, J.B. Nagy, E.G. Derouane, F. Ghigny, in: R. von Balmoos, J.B. Higgins, M.M.J. Treacy (Eds.), Proceedings of the 9th International Zeolite Conference, Montreal, Canada, 1992, Butterworth-Heinemann, Boston, MA, 1993, p. 327.
[2] R.J. Pellet, G.N. Long, J.L. Rabo, P.K. Coughlin, US Patent 4,740,650, 4 (1988).
[3] R.J. Pellet, G.N. Long, J.L. Rabo, P.K. Coughlin, US Patent 4,751,340,6 (1988).
[4] U. Sridevi, N.C. Pradhan, B.K.B. Rao, C.V. Satyanarayana, B.S. Rao, Catal. Lett. 79 (2002) 69–73.
[5] V. Hulea, N. Bilba, M. Lupascu, E. Dumitriu, D. Nibou, S. Lebaili, H. Kessler, Micropor. Mater. 8 (1997) 201–206.
[6] H.O. Pastore, S. Coluccia, L. Marchese, Annu. Rev. Mater. Res. 35 (2005) 351–395.
[7] Y. Wan, D. Zhao, Chem. Rev. 107 (2007) 2821–2860.
[8] K. Egeblad, C.H. Christensen, M. Kustova, C.H. Christensen, Chem. Mater. 20 (2008) 946–960.
[9] W.J. Roth, Stud. Surf. Sci. Catal. 168 (2007) 221–239.
[10] J. Perez-Ramirez, C.H. Christensen, K. Egeblad, C.H. Christensen, J.C. Groen, Chem. Soc. Rev. 37 (2008) 2530–2542.
[11] F.-S. Xiao, Catal. Surv. Asia 8 (2004) 151–159.
[12] H. Wang, T.J. Pinnavaia, Angew. Chem. Int. Ed. 45 (2006) 7603–7606.
[13] Y. Sun, R. Prins, Appl. Catal. A 336 (2007) 11–16.
[14] M. Tiemann, M. Fröba, Chem. Commun. (2002) 406–407.
[15] N. Danilina, F. Krumeich, J.A. van Bokhoven, J. Catal. 272 (2010) 37–43.
[16] M. Choi, H.S. Cho, R. Srivastava, C. Venkatesan, D.-H. Choi, R. Ryoo, Nat. Mater. 5 (2006) 718–723.
[17] C. Baerlocher, W.M. Meier, D.H. Olson, Atlas of Zeolite Framework Types, 5th edition, Elsevier, Amsterdam, 2001.
[18] J.A. Martens, C. Jansens, P.J. Grobet, H.K. Beyer, P.A. Jacobs, in: P.A. Jacobs, R.A. van Santen (Eds.), Zeolites: Facts, Figures Future, Elsevier Sci. Pub., Amsterdam, 1989, p. 215.
[19] H.-X. Li, M.E. Davis, J. Phys. Chem. 96 (1992) 331–334.
[20] X.S. Zhao, G.Q. Lu, A.K. Whittaker, J. Drennan, H. Xu, Micropor. Mesopor. Mater. 55 (2002) 51–62.
[21] L. Wang, C. Guo, S. Yan, X. Huang, Q. Li, Micropor. Mesopor. Mater. 64 (2003) 63–68.
[22] R. Roldan, M. Sanchez-Sanchez, G. Sankar, F.J. Romero-Salguero, C. Jimenez-Sanchidrian, Micropor. Mesopor. Mater. 99 (2007) 288–298.
[23] J.C. Groen, T. Sano, J.A. Moulijn, J. Perez-Ramirez, J. Catal. 251 (2007) 21–27.
[24] J.C. Groen, S. Albello, L.A. Villaescusa, J. Perez-Ramirez, Micropor. Mesopor. Mater. 114 (2008) 93–102.
[25] S. Albello, A. Bonilla, J. Perez-Ramirez, Appl. Catal. A 364 (2009) 191–198.
[26] C.H. Christensen, K. Johannsen, I. Schmidt, C.H. Christensen, J. Am. Chem. Soc. 125 (2003) 13370–13371.
[27] W. Wu, W. Wu, O.V. Kikhtyanin, L. Li, A.V. Toktarev, A.B. Ayupov, J.F. Khabibulin, G.V. Echevsky, J. Huang, Appl. Catal. A 375 (2010) 279–288.
[28] H. Yang, Z. Liu, H. Gao, Z. Xie, Appl. Catal. A 379 (2010) 166–171.
[29] Y.-P. Guo, H.-J. Wang, Y.-J. Guo, L.-H. Guo, L.-F. Chu, C.-X. Guo, Chem. Eng. J. (2010), doi:10.1016/j.cej.2010.10.057.